Supporting information

Elucidating the Sources of Activity and Stability of FeP Electrocatalyst for Hydrogen Evolution Reactions in Acidic and Alkaline Media

Xin Zhao,[a] Zheng Zhang,[b] Xun Cao,[a] Jun Hu,[c,*] Xinghua Wu,[a,d] Andrew Yun Ru Ng,[e] Guo-Ping Lu,[f] Zhong Chen[a,*]

a School of Materials Science and Engineering, Nanyang Technological University, 50 Nanyang Avenue, Singapore 639798, Singapore
b Institute of Materials Research and Engineering, A*STAR (Agency for Science, Technology and Research), #08-03, 2 Fusionopolis Way, Innovis, Singapore 138634, Singapore
c School of Chemical Engineering, Northwest University, Xi'an 710069, P. R. China
d School of Materials & Energy, Guangdong University of Technology, Guangzhou 510006, Guangdong, P. R. China
e Division of Chemistry and Biological Chemistry, School of Physical and Mathematical Sciences, Nanyang Technological University, 21 Nanyang Link, Singapore 637371.
f School of Chemical Engineering, Nanjing University of Science & Technology, Xiaolingwei 200, Nanjing 210094, P. R. China.

E-mail: hujun32456@163.com, ASZChen@ntu.edu.sg

Theoretical calculation details

The CASTEP module of the Materials Studio software (Accelrys Inc.) was employed for the quantum chemistry calculations. The parameter setting are nearly the same as our previous calculation.[1] Self-consistent periodic DFT was adopted by an ultrasoft pseudopotential. Perdew-Burke-Ernzerhof (PBE) approximation was selected as the Generalized Gradient Approximation (GGA) method. And the Broyden-Fletcher-Goldfarb-Shanno (BFGS) scheme was selected as the minimization algorithm. The energy cutoff is set as 380 eV and the SCF tolerance is 1.0×10^{-6} eV/atom. The optimization is completed when the energy, maximum force, maximum stress and maximum displacement are smaller than 5.0×10^{-6} eV/atom, 0.01 eV/Å, 0.02 GPa and 5.0×10^{-4} Å, respectively. During the calculation, FeP (space group 33) was selected with lattice constants a=5.191 Å, b=3.108 Å, and c=5.794 Å. Five low-energy surfaces, viz., the (011), (111), (112), (202), and (211) crystal planes, were selected for the computation. The surfaces were built with a vacuum region of 15 Å. The k-points samplings were set as 2×2×1. The consistent surface energy indicates the method is reasonable, as shown in Figure S1.

Formation energy of the O (P) defect in FeP is calculated using different FeP super-cells. The formation energy of different defects in neutral charge state is defined as:

$$E^{f}_{O(P)} = E^{t}_{bulkO(P)} - E^{t}_{bulk} + E^{t}_{blackP} - 0.5E^{t}_{O_2}$$

$$E^{f}_{O(P)} = E^{t}_{surfaceO(P)} - E^{t}_{surface} + E^{t}_{blackP} - 0.5E^{t}_{O_2}$$

where $E^{t}_{bulk\ O(P)}$, $E^{t}_{surface\ O(P)}$, E^{t}_{bulk}, $E^{t}_{surface}$, $E^{t}_{black\ P}$, $E^{t}_{O_2}$ are the total energies of bulk FeP replacing one P atom by O atom, surface FeP replacing one P atom by O atom, bulk FeP, surface FeP, black P and O_2, respectively.

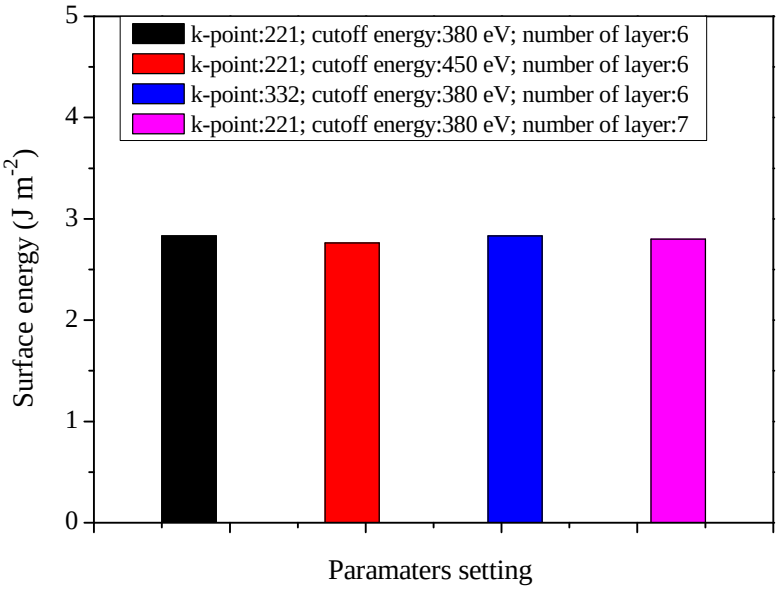

Figure S1. The energy of surfaces with different parameters setting for the (211) facet.

$$\Delta G_H = E[\text{FeP+H}] - E[\text{FeP}] - 1/2E[H_2] + \Delta E_{ZPE} - T\Delta S_H \quad (1)$$

The Gibbs free energy of the adsorption atomic hydrogen is obtained by eq. (1), where *E*[FeP +H] is the total energy of the system, including the adsorbed molecules and the FeP facet; *E*[FeP] is the energy of FeP facet; $E(H_2)$ represents the total energy of a gas phase H_2 molecule, ΔE_{ZPE} denotes the zero-point energy of the system. The term $-T\Delta S_H$ is the contribution from entropy at temperature K.[2]

$$\Delta E_{surface} = 0.5(E[\text{FeP}] - nE[\text{bulk FeP}])/A \quad (2)$$

The surface energy calculated by eq. (2), where *n* is the number of Fe atom on the surface, *E*[bulk FeP] is the total energy of one FeP for bulk FeP. A is the surface area of the surface model.

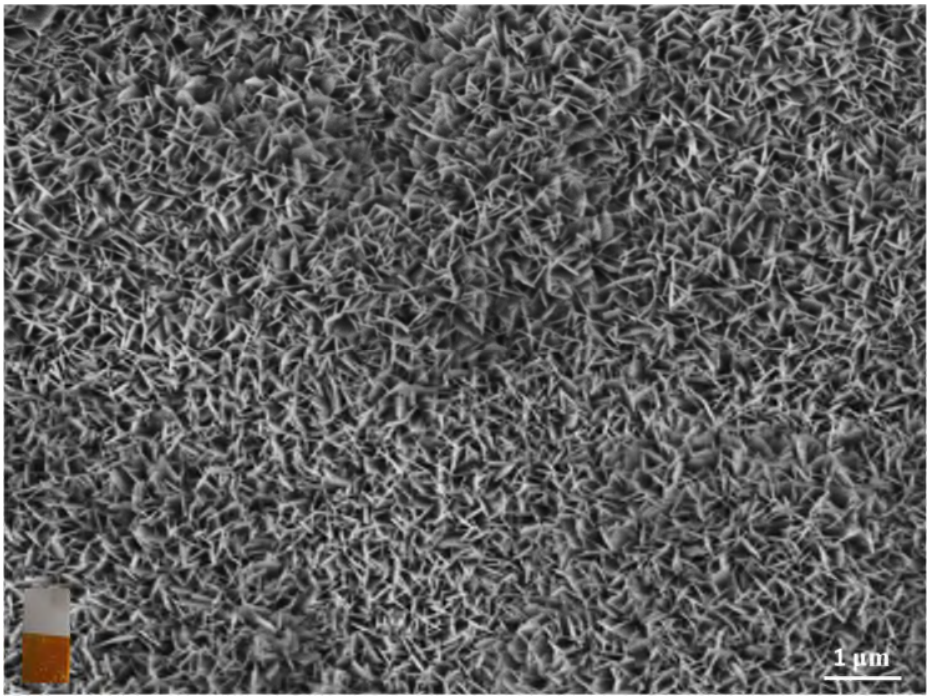

Figure S2. SEM image of the prepared FeOOH film. Inset is the digital photo of the as synthesized FeOOH/Ti.

Table S1. The Fe and P content in FeP by EDX.

Element	wt%	at%
Fe	63.06	48.64
P	36.94	51.36

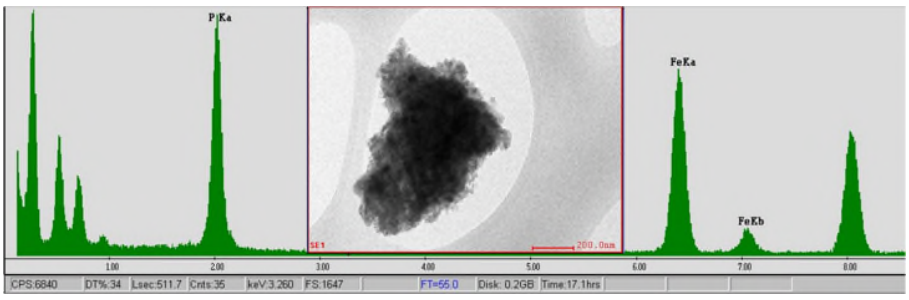

Figure S3. EDS spectra of FeP.

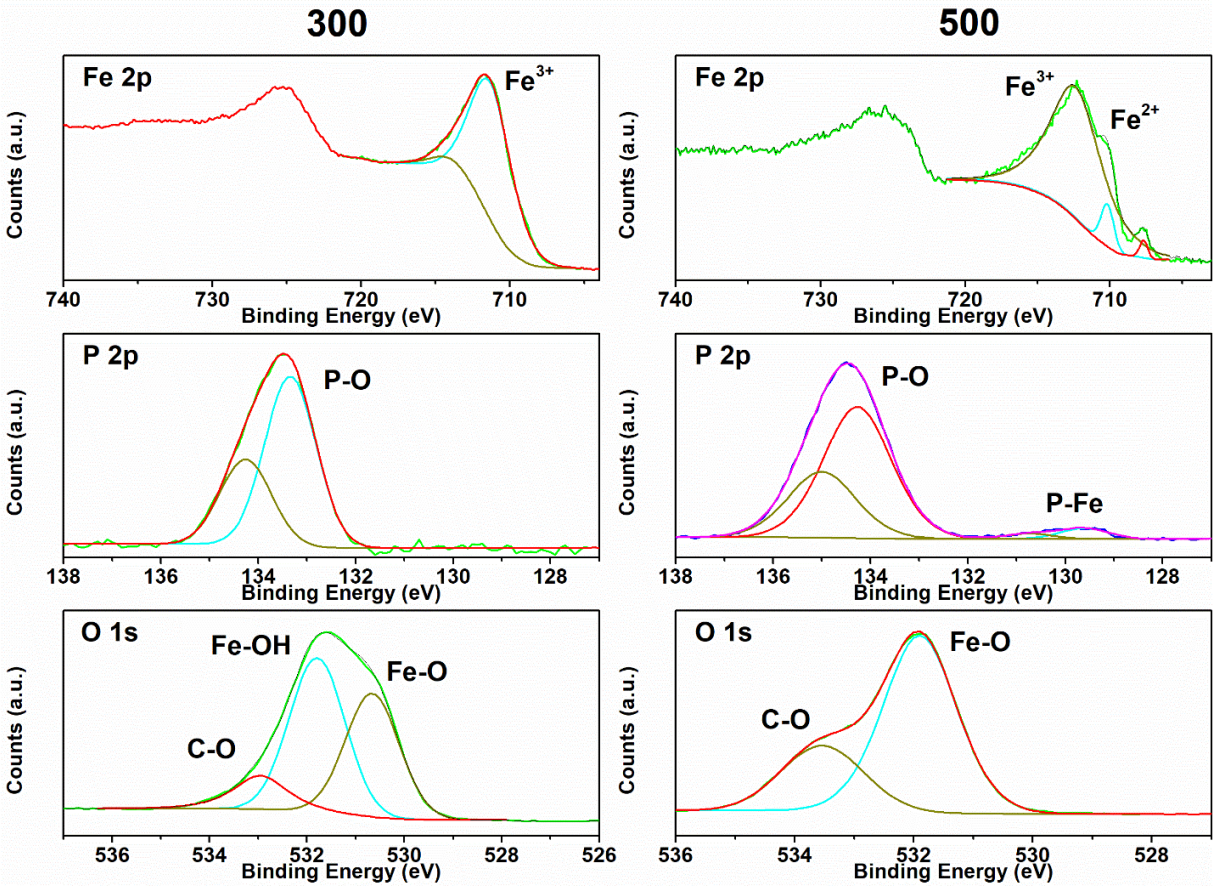

Figure S4. XPS spectra of Fe 2p, P 2p, and O 1s for FeP synthesized at 300 and 500°C.

XPS spectra show that at the low temperature (300°C), no obvious Fe-P bond was formed. The surface is mostly composed of FeOOH and iron phosphate. In contrast, at 500°C, peaks of Fe-P bond started to become prominent. It is interesting to note that there are more Fe-P bonds at 400°C than 500°C based on the bond intensity. This is because it is more likely to form Fe-O oxide other than FeP at high temperatures.

Table S2 Element content analysis of FeP synthesized at 400 and 500°C by XPS.

Elements	400°C		500°C	
	Peak Binding Energy (eV)	Composition (at%)	Peak Binding Energy (eV)	Composition (at%)
$P2p_{3/2}$ FeP	129.7	3.2	129.6	1.2
$P2p_{3/2}$ $(PO4)^{3-}$	133.8	16.8	134.3	21.3

C1s C-C/C-H	285.0	10.4	285.0	12.2
C1s C-O	286.8	3.0	286.7	3.6
C1s O-C=O	289.3	1.1	289.4	1.9
O1s O-Fe	-	-	-	-
O1s O-P/Fe-OH/O-Fe	531.9	37.7	531.9	38.7
O1s O-C	533.1	24.0	533.5	15.6
$Fe2p_{3/2}$ FeP	707.6	0.7	707.7	0.1
$Fe2p_{3/2}$ Fe-O	709.8	0.3	710.2	0.6
$Fe2p_{3/2}$ Fe-O	712.6	2.8	712.4	4.9

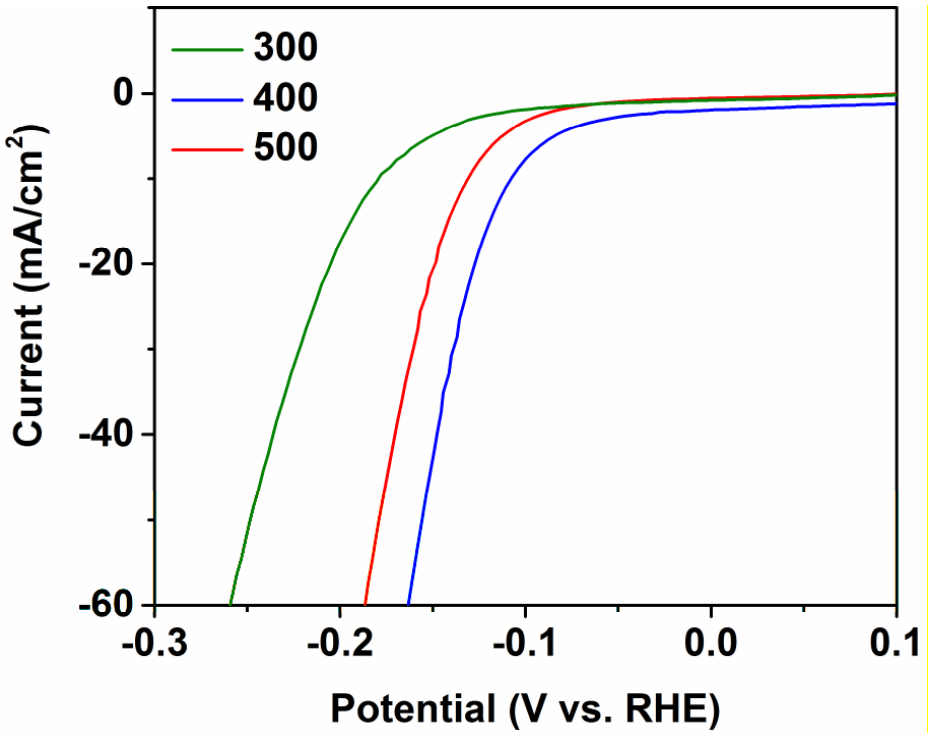

Figure S5. The LSV test of HER of FeP synthesized at 300, 400, 500°C in alkaline solution.

Table S3 Relative content of oxygen by the XPS measurement of P-O and P-Fe content in the FeP synthesized at 300, 400 and 500°C.

Synthesis temperature (°C)	P-Fe (%)	P-O (%)	ratio of P-O / P-Fe
300	0	6.9	∞
400	3.2	16.8	8.4
500	1.2	21.3	17.7

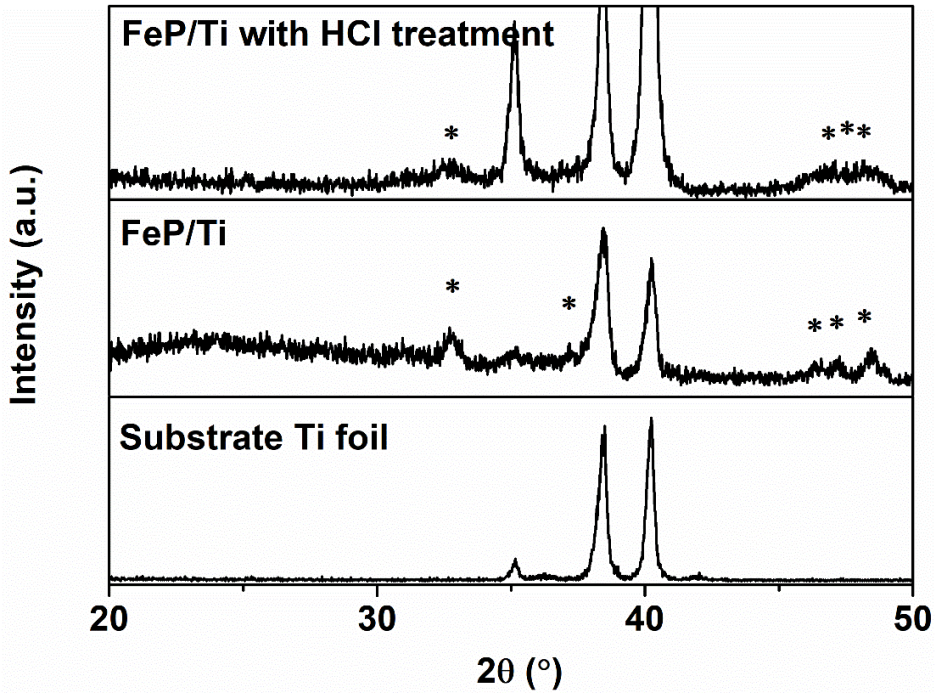

Figure S6. XRD patterns of FeP/Ti after HCl treatment. Substrate Ti foil and FeP/Ti without HCl treatment were also listed for comparison.

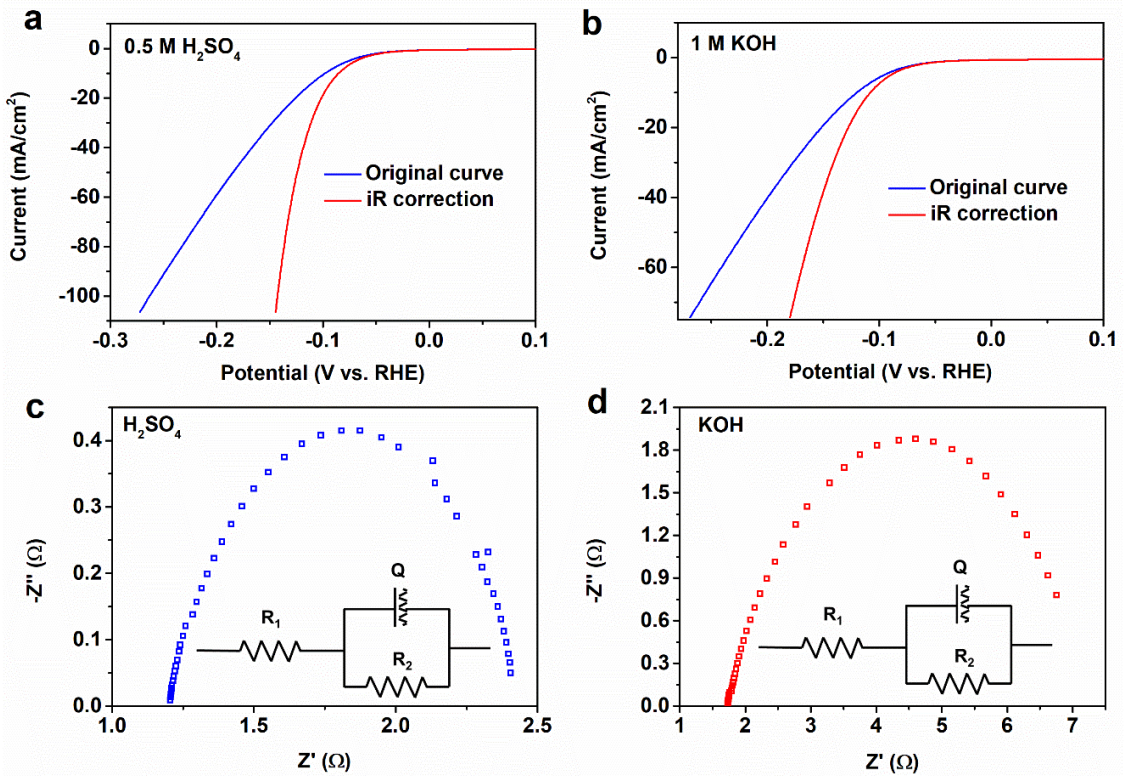

Figure S7. Comparison of LSV polarization curves of FeP/Ti in (a) acid (0.5 M H_2SO_4) and (b) alkaline (1 M KOH) electrolyte for HER with and without iR compensation. EIS at -0.1 V vs RHE for FeP test in (c) 0.5 M H_2SO_4 and (d) 1 M KOH. The insets in (c) and (d) are the equivalent circuits to simulate the EIS.

Table S4. Fitting data using equivalent circuits in Figure S7 (c) and (d) by simulating the EIS data in Figure S7 (c) and (d).

	H_2SO_4	**KOH**
R1 (Ω)	1.2	1.7
Q ($S\ s^n$)	0.068	0.055
n	0.78	0.8
R2 (Ω)	1.2	5.26

Table S5. HER performance of FeP reported.

Catalyst	Electrolyte	η_{10} (mV vs. RHE)	Tafel slope (mV dec^{-1})	Reference
FeP nanosheets	0.5 M H_2SO_4	~240	67	[3]
FeP NA/Ti	0.5 M H_2SO_4	55	38	[4]
FeP NAs/CC	0.5 M H_2SO_4	58	45	[5]
	1 M KOH	218	146	
FeP NAs/Ti	0.5 M H_2SO_4	85	60	[6]
FeP/CC	0.5 M H_2SO_4	39	32	[7]
FeP-GS	0.5 M H_2SO_4	123	50	[8]
FeP NRs	0.5 M H_2SO_4	120	55	[9]
FeP NWs/rGO	0.5 M H_2SO_4	107	58	[10]
FeP Nanotubes	0.5 M H_2SO_4	88	35.5	[11]
	1 M KOH	120	59.5	
FeP/CC	0.5 M H_2SO_4	34	29	[12]
FeP-CS	0.5 M H_2SO_4	112	58	[13]
FeP array	0.5 M H_2SO_4	96	39	[14]
	1 M KOH	194	75	
HMFeP@C	0.5 M H_2SO_4	115	56	[15]
Carbon shell-coated FeP/C	0.5 M H_2SO_4	71	52	[16]
FeP NR/Ti	0.5 M H_2SO_4	70	39	[17]
hollow FeP microspheres	0.5 M H_2SO_4	144	58	[18]
FePNRs/VAGNs/CC	0.5 M H_2SO_4	53	42	[19]
FeP@OMC/CC	0.5 M H_2SO_4	51	39	[20]
Petaloid FeP/C	0.5 M H_2SO_4	110	57	[21]
	1 M KOH	185	93	
FeP/GA	0.5 M H_2SO_4	150	65	[22]
	1 M KOH	240	142	
Ni-doped FeP/C	0.5 M H_2SO_4	72	54	[23]
	1 M KOH	~100	72	
Ni-doped FeP/TiN/CC	1 M KOH	75	73	[24]
FeP nanosheet/Ti	0.5 M H_2SO_4	79	58	This work
	1 M KOH	95	64	

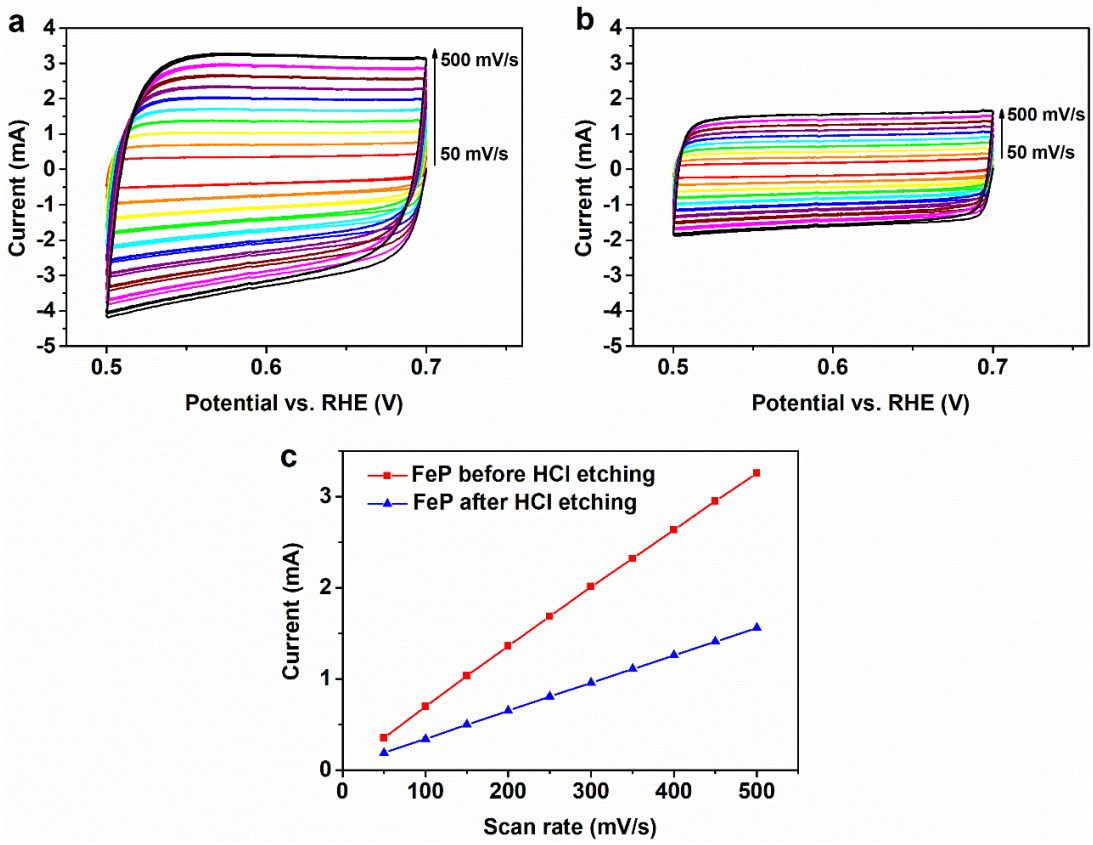

Figure S8. Electrocatalytically active surface area (ECSA): Cyclic voltammograms (CV) measured for the FeP (a) before HCl etching and (b) after HCl etching at 10 different scan rates. (b) The linear relationship between the capacitive current at 0.76 V vs. RHE vs. varying scan rates.

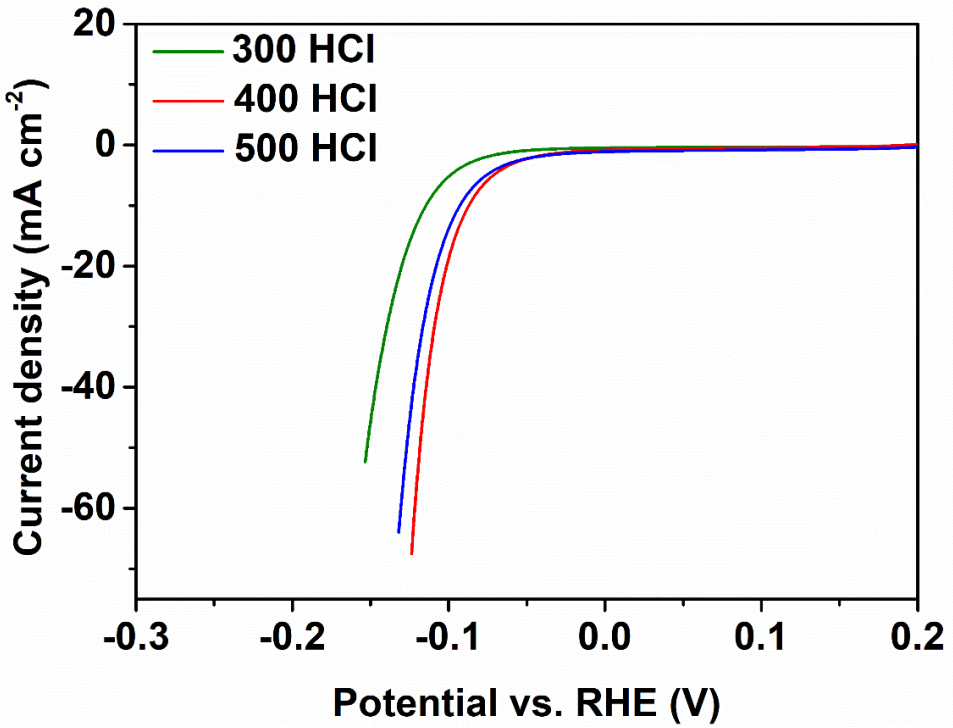

Figure S9. The HER of FeP synthesized at 300, 400, and 500°C after HCl etching tested in alkaline condition.

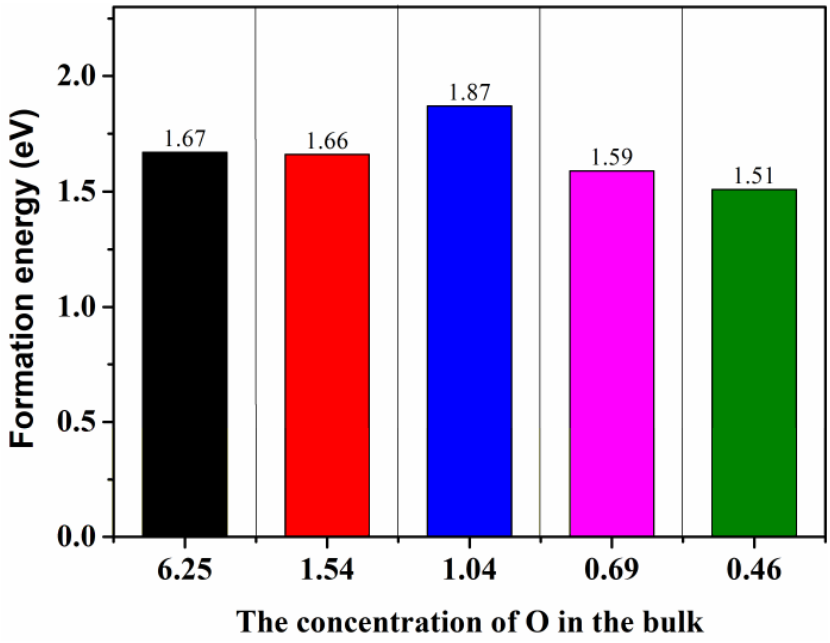

Figure S10. Formation energy of bulk P substituted by O atoms.

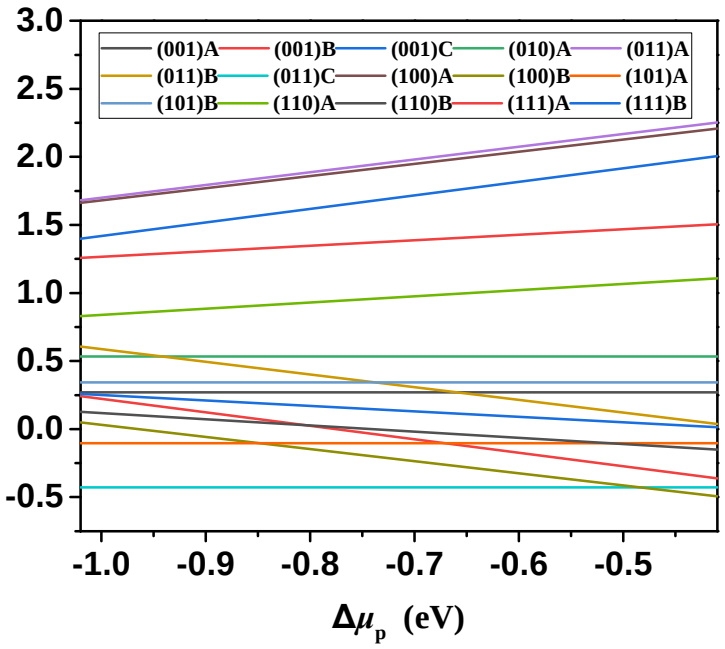

Figure S11. Surface energy of low index facets. A, B and C represent different terminated position of different surfaces.

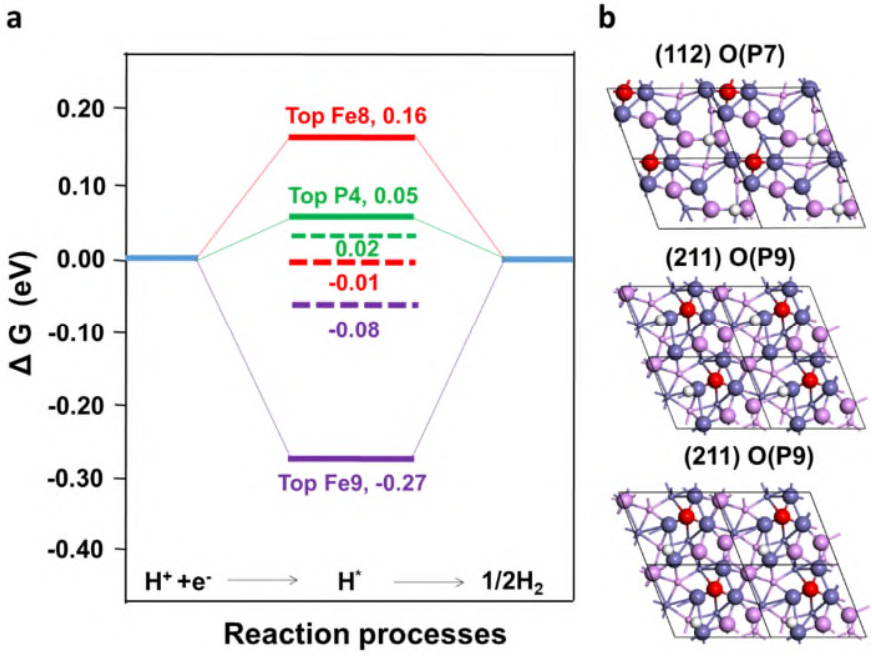

Figure S12. (a) Gibbs free energies profile of H_2 generation on different active P and Fe sites on (112) and (211) facets after replacing P atom with O atom; (b) Top view of replacing sites and reaction sites on different surfaces for calculation of Gibbs free energies. Violet spheres stand for P atoms, blue spheres stand for Fe atoms, red spheres stand for O atoms and white spheres stand for H atoms.

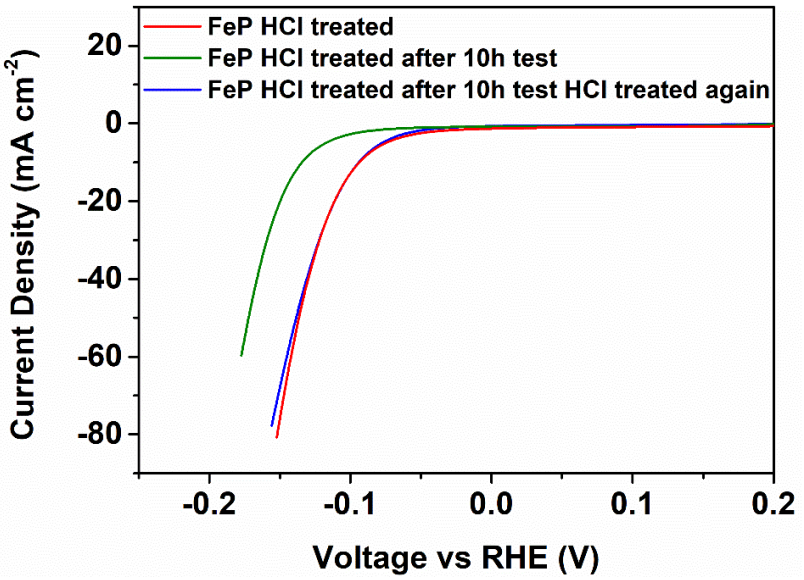

Figure S13. The comparison of HER performance of FeP treated with HCl and after stability test with HCl treatment again.

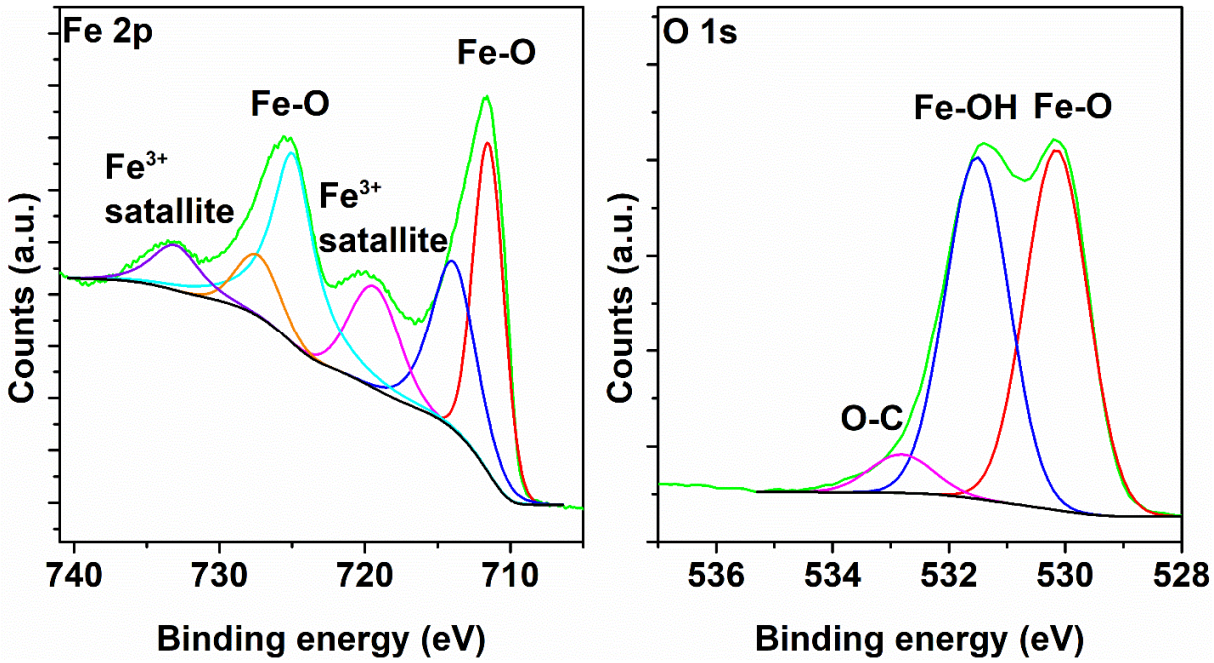

Figure S14. XPS spectra of Fe 2p and O 1s for FeOOH.

Table S6. Theoretical calculations and corresponding enthalpy change ΔH of the possible reactions of FeP in alkaline with and without presence of oxygen.

Presence of O_2 (YES or NO)	Reaction	Calculated ΔH (kJ mol^{-1})
Y	$4FeP + 12KOH + 7O_2 \rightarrow 2H_2O + 4K_3PO_4 + 4Fe(OH)_2$	-5541
Y	$FeP + 3KOH + 2O_2 \rightarrow H_2O + K_3PO_4 + FeOOH$	-1510
Y	$4FeP + 20KOH + 11O_2 \rightarrow 10H_2O + 4K_3PO_4 + 4K_2FeO_4$	-6192
N	$2FeP + 6KOH + 6H_2O \rightarrow 7H_2 + 2K_3PO_4 + 2Fe(OH)_2$	47
N	$FeP + 3KOH + 3H_2O \rightarrow 4H_2 + K_3PO_4 + FeOOH$	100
N	$2FeP + 10KOH + 6H_2O \rightarrow 11H_2 + 2K_3PO_4 + 2K_2FeO_4$	1332

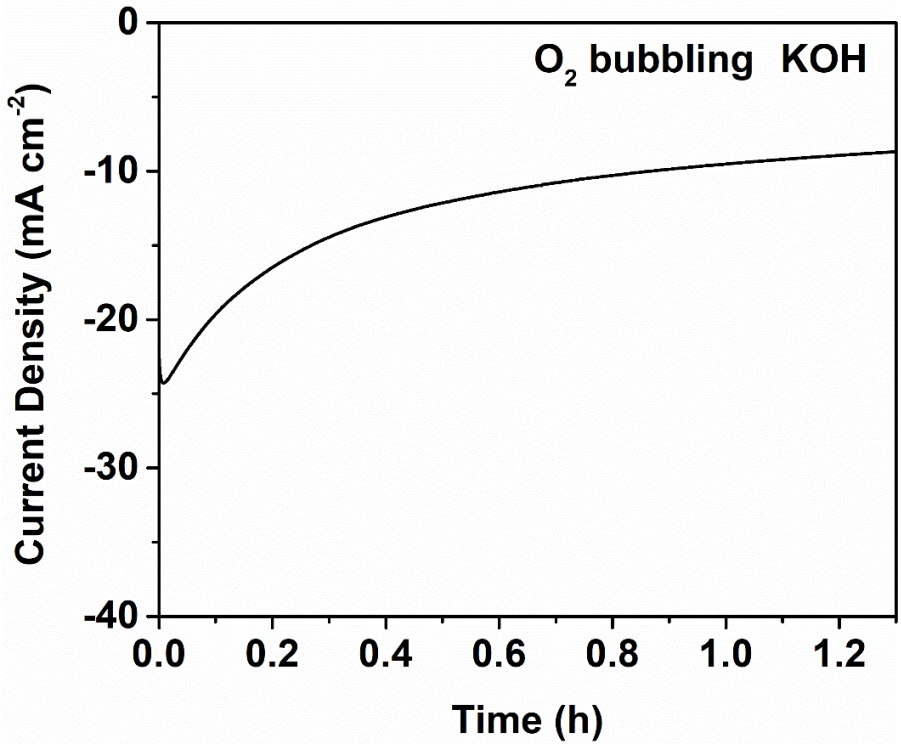

Figure S15. Stability for the HER in 1 M KOH electrolyte with gentle bubbling of O_2 during the test.

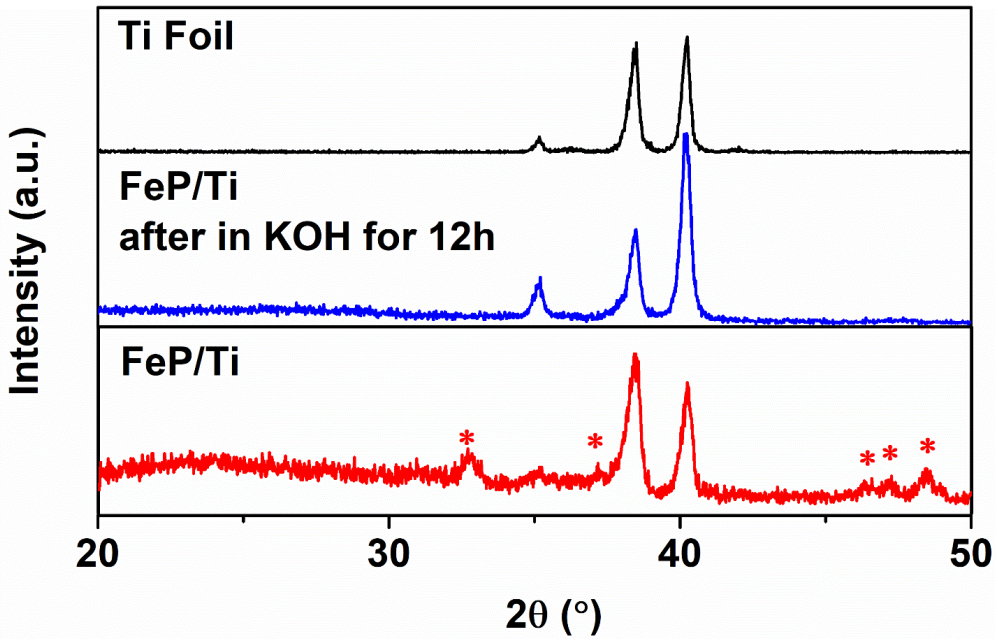

Figure S16. XRD patterns of FeP/Ti after soaking in 1 M KOH for 12h. XRD patterns of substrate Ti foil and FeP/Ti were given for comparison.

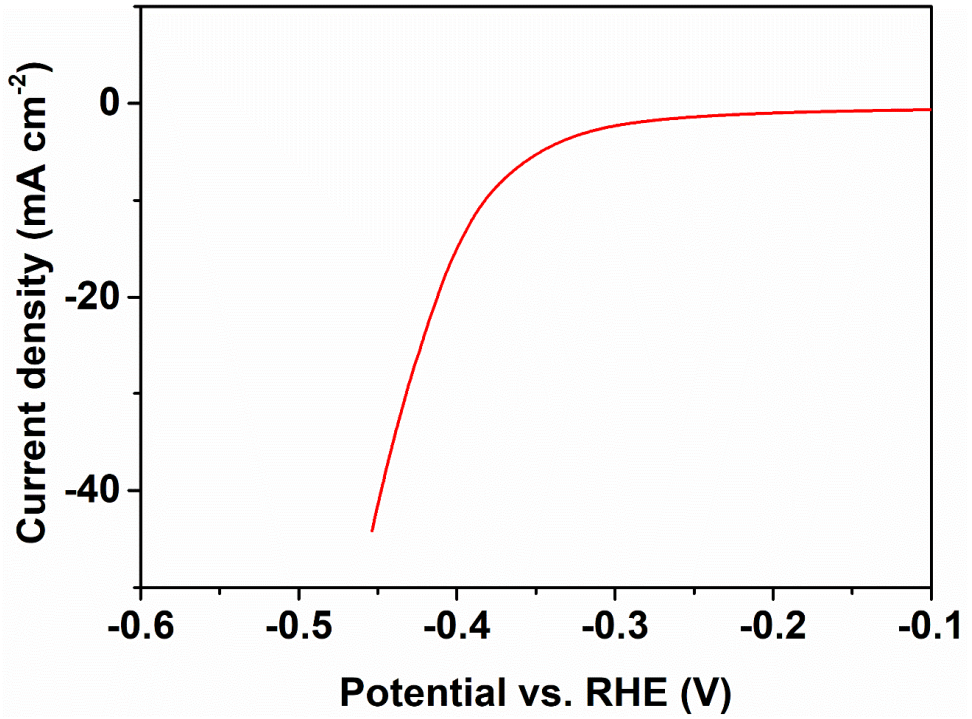

Figure S17. The HER performance of FeP treated with HCl tested in 0.5 M K_2SO_4 (pH is tuned to 7 by adding a little amount of 1M KOH solution).

References

[1] J. Hu, S. Zheng, X. Zhao, X. Yao and Z. Chen, J. Mater. Chem. A, 2018, 6, 7827-783
[2] Q. Tang, D.-e. Jiang, Acs Catal., 6 (2016) 4953-4961.
[3] Y. Xu, R. Wu, J. Zhang, Y. Shi, B. Zhang, Chem. Commun., 49 (2013) 6656-6658.
[4] P. Jiang, Q. Liu, Y. Liang, J. Tian, A.M. Asiri, X. Sun, Angew. Chem., 126 (2014) 13069-13073.
[5] Y. Liang, Q. Liu, A.M. Asiri, X. Sun, Y. Luo, Acs Catal., 4 (2014) 4065-4069.
[6] R. Liu, S. Gu, H. Du, C.M. Li, J. Mater. Chem. A, 2 (2014) 17263-17267.
[7] J. Tian, Q. Liu, Y. Liang, Z. Xing, A.M. Asiri, X. Sun, ACS Appl. Mater. Inter., 6 (2014) 20579-20584.
[8] Z. Zhang, B. Lu, J. Hao, W. Yang, J. Tang, Chem. Commun., 50 (2014) 11554-11557.
[9] H. Du, S. Gu, R. Liu, C.M. Li, Int. J. Hydrogen Energy, 40 (2015) 14272-14278.
[10] Y. Yan, L. Thia, B.Y. Xia, X. Ge, Z. Liu, A. Fisher, X. Wang, Adv. Sci., 2 (2015) 1500120.
[11] Y. Yan, B.Y. Xia, X. Ge, Z. Liu, A. Fisher, X. Wang, Chem. Eur. J., 21 (2015) 18062-18067.
[12] X. Yang, A.-Y. Lu, Y. Zhu, S. Min, M.N. Hedhili, Y. Han, K.-W. Huang, L.-J. Li, Nanoscale, 7 (2015) 10974-10981.
[13] Z. Zhang, J. Hao, W. Yang, B. Lu, J. Tang, Nanoscale, 7 (2015) 4400-4405.
[14] C.Y. Son, I.H. Kwak, Y.R. Lim, J. Park, Chem. Commun., 52 (2016) 2819-2822.
[15] X. Zhu, M. Liu, Y. Liu, R. Chen, Z. Nie, J. Li, S. Yao, J. Mater. Chem. A, 4 (2016) 8974-8977.
[16] D.Y. Chung, S.W. Jun, G. Yoon, H. Kim, J.M. Yoo, K.-S. Lee, T. Kim, H. Shin, A.K. Sinha, S.G. Kwon, J. Am. Chem. Soc., 139 (2017) 6669-6674.
[17] J. Gao, P. Luo, H. Qiu, Y. Wang, Nanotechnology, 28 (2017) 105705.
[18] X. Guo, Z. Feng, Z. Lv, Y. Bu, Q. Liu, L. Zhao, C. Hao, G. Li, Q. Lei, ChemElectroChem, 4 (2017) 2052-2058.
[19] D. Li, Q. Liao, B. Ren, Q. Jin, H. Cui, C. Wang, J. Mater. Chem. A, 5 (2017) 11301-11308.
[20] Z. Liu, Z. Gao, F. Luo, S. Yuan, K. Wang, N. Li, X. Li, ChemCatChem, 10 (2018) 3441-3446.
[21] F. Wang, X. Yang, B. Dong, X. Yu, H. Xue, L. Feng, Electrochem. Commun., 92 (2018) 33-38.
[22] N.K.A. Venugopal, S. Yin, Y. Li, H. Xue, Y. Xu, X. Li, H. Wang, L. Wang, Chem. Asian J., 13 (2018) 679-685.
[23] X.F. Lu, L. Yu, X.W.D. Lou, Sci. Adv., 5 (2019) 6009.
[24] X. Peng, A.M. Qasim, W. Jin, L. Wang, L. Hu, Y. Miao, W. Li, Y. Li, Z. Liu, K. Huo, Nano Energy, 53 (2018) 66-73.